A new azine-based ferrocenophane for azo dyes degradation in dark–ambient conditions

Shahriar Sharifi [a], A. Wahid Mesbah [a,*], Somayeh Golsanamlou [a], Aliakbar Tarlani [a], Mitra Ghassemzadeh [a], Effat Iravani [b], Olaf Fuhr [c], Dieter Fenske [c]

[a] Chemistry and Chemical Engineering Research Center of Iran, Pajoohesh Blvd., 17th Km of Tehran–Karaj Highway, Tehran 14968-13151, Iran
[b] Nuclear Science and Technology Research Institute, Tehran, Iran
[c] Institut Für Nanotechnologie and Karlsruhe Nano Micro Facility (KNMFi), Karlsruher Institut für Technologie, Kaiserstraße 12, Karlsruhe 76131, Germany

Keywords:
Ferrocenyl azine
Congo red degradation
Dark-ambient degradation
Azo dyes
Advanced oxidation process

A B S T R A C T

In a novel approach, 1,1′-bis(2,3-diazabuta-l,3-dien)ferrocenophane (Fc-azine) synthesized by self-condensation of 1,1′-Ferrocenedicarboxaldehyde hydrazone (FcDH) with the aid of $Zn(OAc)_2{\cdot}2H_2O$ or acetic acid at 120 °C under high pressure. Fc-azine as an insoluble compound was fully characterized by Fourier transform infrared spectroscopy (FT-IR), diffuse reflectance spectroscopy (DRS), thermogravimetric analysis (TGA), Brunauer-Emmett-Teller analyses (BET), powder x-ray diffraction (XRD) and single crystal x-ray diffraction. The narrow band gap (Eg 1.93 eV) and the presence of ferrocene and azine functional groups encouraged us to use Fc-azine as an advanced oxidation process (AOP) catalyst. Interestingly, the addition of Fc-azine (1 g L^{-1}) to aqueous solutions of 50 ppm of Congo red (CR) and 10 ppm of methyl orange (MO) led to the fast degradation of CR (over 80 % in 5 min) and the slow degradation of MO (98 % in 48 h) in the dark, without additional energy sources or chemical reagents. It was found that Fc-azine can degrade CR in six cycles with high efficiency (over 80 %). CR degradation by Fc-azine can be performed in acid and basic environments (pH 3–9), and effective MO degradation happens in slightly acidic and natural environments (pH 5–7). Possible adsorption, reactive oxygen species production (·OH, $O_2{\cdot}^-$), and the mechanism of CR and MO degradation were also studied.

1. Introduction

With industrialization and population growth during the last centuries, water pollution, like soil and air pollution, has become a tremendous environmental problem [1–4]. Among all chemical pollutants, dyes with over 10,000 known types, 700,000 tons/year of production, and 280,000 tons/year of discharge to surface water are among the major wastewater problems [5]. Azo dyes comprise more than 60 % of all dyes productions widely used in textile industries [6]. Azo dyes are mainly non-biodegradable, decompose to toxic and carcinogenic byproducts, and affect water transparency and aquatic photosynthesis even in small amounts (1 ppm) [7,8]. Azo dyes could be physically removed by adsorption, coagulation-flocculation, ion exchange, and membrane filtration without degradation [9,10]. Unfortunately, these methods need downstream treatment and suffer from low efficiency, high cost, and poor adsorbent recovery [11,12].

Chemical and biological degradations are other approaches for dye treatment of wastewater. The biological degradation has low efficiency [13,14] and can lead to the production of toxic aromatic amines [15]. Advanced oxidation process (AOP) is an effective chemical degradation method for chemical effluents and dyes. AOPs process consists of producing highly reactive oxygen species (·OH, $O_2{\cdot}$ and $^1O_2$), which can mineralize organic effluent to non-toxic or less toxic products such as CO_2, H_2O, and salts [16,17]. Thus, an optimal AOP could resolve defects of adsorption and biological methods for azo-dyes removal. Fenton reaction, ozonization, and photocatalytic reactions are the most known AOPs. Ozonization and Fenton reactions mainly need additional chemical reagents (O_3 and H_2O_2) and special conditions (acidic medium for Fenton reaction), which make them expensive and challenging to perform [4]. Photocatalytic properties of TiO_2 were discovered for the first time by Fujishimna and Honda in 1972 [18]. Due to the low quantum yield and wide band gap (3.2 eV) of TiO_2, many researchers have studied the modification of TiO_2 for better photocatalytic activity [19–21].

Many other photocatalysts based on semiconductors, such as metal oxides, metal-organic frameworks, and metal complexes, have been

* Corresponding author.
E-mail address: mesbah@ccerci.ac.ir (A.W. Mesbah).

reported [22–26]. Despite the simple operation of photocatalysts, sometimes they also need some other chemical reagents such as H_2O_2. Furthermore, photocatalysts are only activated by sunlight or other light emission sources. Some exciting research has been published based on day-night photocatalysts, a composite of a semiconductor photocatalyst and an electron storage compound. In these types of photocatalysts, light emission provides photocatalyst activity and photo-charge; then, dark discharge can continue the AOP process in the absence of an emission source. Despite the advantages of day-night catalysts, their preparation, electron storage capacity, and discharge rate for maintaining AOP need more investigation [12].

Defects and conflicts of photocatalysts create a necessity for AOP catalysts that can run at ambient conditions without external energy (light, heat, or ultrasonication) or chemical reagents for wastewater treatment. Several of these types of catalysts based on modified perovskite, metal chalcogenide, metal oxide, and nanocomposites have been reported [3]. Most dark AOP catalysts have species with a small band gap ($E_g < 2.5$ eV), which can provide highly reactive radicals at ambient conditions. For instance, Chen et al. reported calcium strontium copper perovskites ($Ca_xSr_{1-x}CuO_{3-\delta}$) for fast degradation of Orange II (10–100 ppm) up to 80 % within 10 min [5]. Besegatto et al. prepared the Ca-Ni-Fe-based perovskite-like structures ($CaNi_xFe_{(1-x)}O_{3-\delta}$) with high reactivity for degradation of Reactive Red 141 and Acid orange II (20 ppm) with over 50 % dye removal in 10 min [17]. An orthorhombic tin monosulphide nanocatalyst was reported by Jayaraman et al. with high activity (up to 99 %) for degradation of Methylene blue (MB), Congo red (CR), and Eriochrome black T (40 ppm) [27]. A number of nanocomposites also have been used for azo dye degradation in the dark. For instance, Prasanna and coworkers reported ZnO_2/polypyrrole nanoparticles for degradation of MB (5 ppm) and Rhodamine B (10 ppm) in 10 min [9]. Very recently, Molahosseini and coworkers reported that Fe_3O_4/MWCNT/SiO_2 magnetic nanocomposite could ultra-fast degrade MB in 30 s [11]. Modified TiO_2/polypyrrole, Cu_2O nanocomposite [28], and $MgFe_2O_4$ [29] are other successful examples of AOP catalysts in the dark for azo dye removal.

It has been reported that ferrocene can enhance the activity of AOP photocatalysts by facilitating radical production through the oxidation of Fe(II) to Fe (III), modifying the band gap of the catalyst and electron-donating properties [30–35]. In addition, a reported π-conjugated phenylazine polymer has shown effective photocatalytic degradation of the organic compounds [36]. Therefore, Fc-azine, as a ferrocenophane containing azine and ferrocenyl groups with high thermal stability (decompose at ~300 °C), insolubility and narrow band gap, was studied as an AOP catalyst for azo dye degradation. Fc-azine has shown high and moderate activity for CR (50 ppm) and MO (10 ppm) degradation, respectively, in the dark without using chemical reagents or external energy. Based on our literature review, Fc-azine is the first metallocene utilized to degrade azo dyes in the dark.

2. Experimental

2.1. Materials and instrumentation

1,1′-Ferrocenedicarboxaldehyde was synthesized based on the reported literature [37]. Other reagents were purchased from commercial resources and used without further purification, except for n-butyllithium, which was prepared freshly in the lab. All solvents were purified by standard procedures.

The ^{1}HNMR spectra were acquired using a Varian INOVA-500 MHz spectrometer. Chemical shifts (δ) were reported in parts per million (ppm) using TMS as an internal standard and DMSO-d6 as deuterated solvents. FT-IR spectra were obtained on a Perkin-Elmer 400 Spectrometer. DRS and UV–Vis spectra were recorded using a PerkinElmer Lambda 35 Spectrophotometer. GCMS– data was obtained by Varian 320-MS GC/MS. TGA diagram measured by NETZSCH Perseus TG 209 F1. The measurement of the BET (Brunauer-Emmett-Teller) plot was conducted using a BELSORP mini II lab analyzer. The XRD analysis was performed using the Philips PW 1730 instrument at an angle between 10 and 80°. EDX analysis was performed by the TESCAN Vega model 3 microscope with an accelerating voltage of incident electrons equal to 30 keV using a silicon drift detector (Oxford Instruments). Zeta-potential measurement was assessed by an electro-kinetic analyzer, which measured the surface charges of Fc-azine. The surface morphology was observed using a field-emission scanning electron microscope (FE-SEM, MIRA III TESCAN) equipped with an energy-dispersive X-ray analysis (EDS) system.

Table 1
Crystal data and structure refinement for Fc-azine.

Emp. formula	$C_{24}H_{20}Fe_2N_4$
Formula mass	476.14
Crystal system	monoclinic
Space group	$P2_1/c$
Temperature [K]	180
a [Å]	9.4034(2)
b [Å]	10.3653(2)
c [Å]	10.5165(3)
α [°]	90
β [°]	113.867(2)
γ [°]	90
Volume [Å^3]	937.38(4)
Z	2
D_{calc} [g cm ^{3}]	1.687
μ [mm^{-1}]	8.449
F(000)	488.0
Crystal size [mm]	0.16 × 0.03 × 0.02
Radiation	GaKα (λ = 1.34143)
2θ range for data collection/°	8.946 to 124.96
Reflections collected	14050
Independent reflections	2261 [R_{int} = 0.0350, R_{sigma} = 0.0191]
Data/restraints/parameters	2261/0/136
Goodness-of-fit on F^2	1.059
Final R indexes [I ≥ 2σ (I)]	R_1 = 0.0287, wR_2 = 0.0780
Final R indexes [all data]	R_1 = 0.0332, wR_2 = 0.0798[a]
Largest diff. peak/hole /e Å ^{3}	1.10/-0.46

[a] w $1/[\sigma^2(Fo^2) + (0.0533.P)^2 + (0.2661.P)]$; P $[\max(Fo^2, 0) + 2.Fc^2]/3$.

Single crystal X-ray diffraction data of Fc-azine were collected on a STOE StadiVari diffractometer with monochromated Ga Kα (1.34143 Å) radiation at 180 K. Using Olex2 [38], the structures were solved with the ShelXT [39] structure solution program using Intrinsic Phasing and refined with the ShelXL [40] refinement package using Least Squares minimization. Refinement was performed with anisotropic temperature factors for all non-hydrogen atoms; hydrogen atoms were calculated on idealized positions. Crystallographic data and refinement details are summarized in Table 1.

2.2. Synthesis of 1,1′-Ferrocenedicarboxaldehydehydrazone (FcDH)

Under an argon atmosphere, 1,1′-Ferrocenedicarboxaldehyde (1.65 mmol, 0.4 g) dissolved in methanol (10 mL) and was added dropwise to a solution of hydrazinemonohydrate (12.34 mmol, 0.6 mL) in methanol (5 mL). The reaction mixture was stirred for 16 h, and volatiles were removed under a high vacuum. FcDH was obtained as an orange powder (0.41 g, 90 % yield), characterized, and used in the next reactions without further purification. The highly reactive FcDH should be kept in an argon atmosphere at -20 °C to avoid room-temperature decomposition.

FT-IR (cm ^{1}): 1628, (C=N), 3370 and 1587 (N-H). ^{1}HNMR (500 MHz, DMSO-d_6) δ = 4.19 (s, 4H, C_4H_5), 4.37 (s, 4H, C_5H_4), 6.18(s, 4H, NH_2), 7.31 (s, 2H, CH=N).

2.3. Synthesis of 1,1′-bis(2,3-diazabuta-l,3-dien)ferrocenophane (Fc-azine)

The solution of zinc acetatedihydrate (0.73 mmol, 0.16 g) in

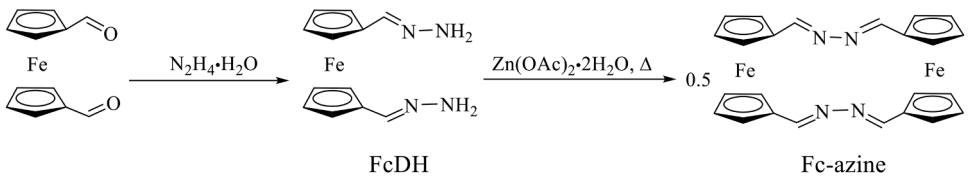

Scheme 1. Synthesis of FcDH and Fc-azine.

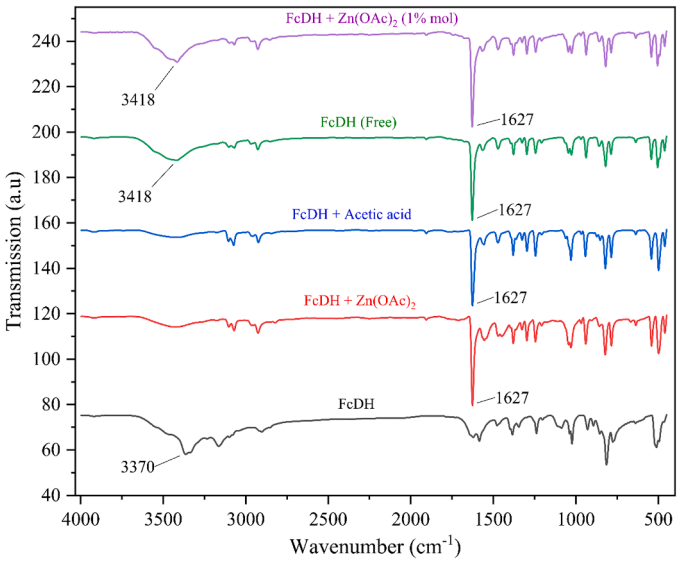

Fig. 1. FT-IR spectra of different reactions of FcDH at 120 °C in methanol.

methanol (5 mL) was added to a 15 mL methanolic solution of FcDH (0.73 mmol, 0.2 g). The reaction mixture was stirred for 3 min, transferred into a hydrothermal autoclave reactor, and kept at 120 °C for 14 h. The resulting dark-red crystals of Fc-azine were washed several times with methanol and dried at room temperature (0.14 g, 81 % yield). Fc-azine is insoluble in common organic solvents and was characterized by DRS, BET, FT-IR, TGA, XRD analyses, and single crystal x-ray diffraction. FT-IR (cm ^{1}): 1627 (C=N), decomposed at 300 °C.

2.4. *Catalytic degradation procedure*

To a 100 mL solution of CR with an initial concentration of 50 ppm, 0.1 g of Fc-azine was added. The reaction mixture was stirred (500 rpm) in a dark box at room temperature and pH= 7. The degradation process was monitored by tanking out 1 mL samples in desired time intervals. To evaluate catalyst reusability, 5 mL of solution was taken out every 2 h and replaced by 5 mL of 1000 ppm of CR solution. Every sample was centrifuged, and CR concentration was obtained from Eq. (1) using the UV–Vis spectrum at λ = 498 nm. A similar method was performed for MO degradation with an initial concentration of 10 ppm.

$$\text{Dye degradation efficiency } (\%) = \frac{C_0 \quad C}{C_0} \times 100 \qquad (1)$$

C_0 is the initial dye concentration, and C is the concentration calculated from the UV-Vi spectra of each sample.

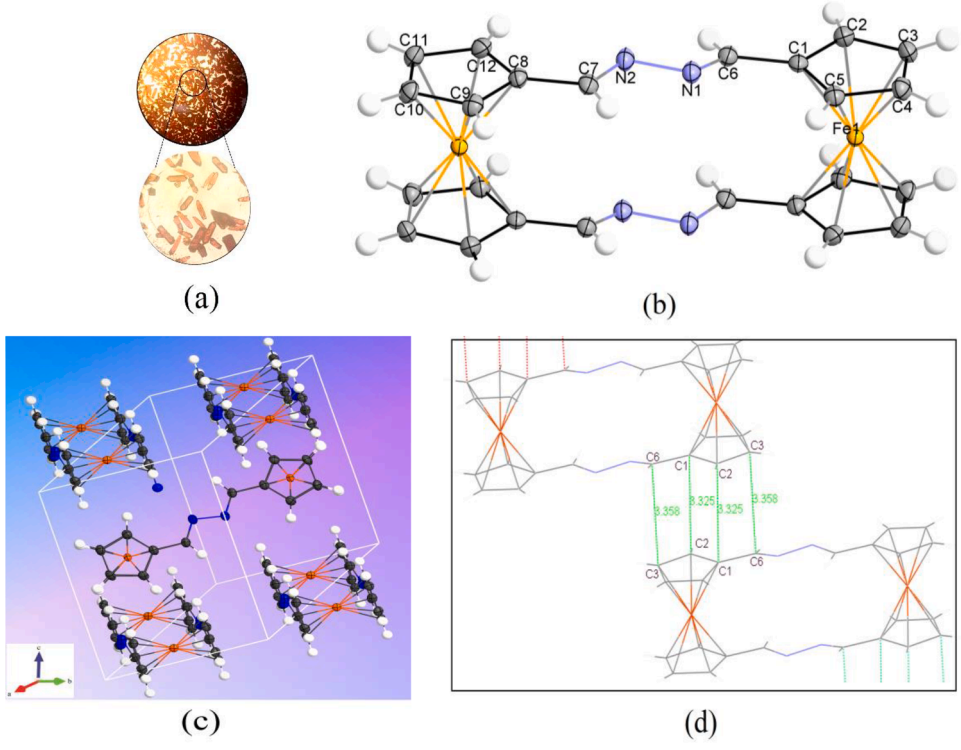

Fig. 2. (a) optical microscope image of Fc-azine crystals, (b) molecular structure of Fc-azine (thermal ellipsoids are depicted at the 50 % probability level), (c) unite cell and eclipsed conformation of Cp rings of Fc-azine, and (d) distances between atoms containing possible π-π interaction.

Table 2
selected bonds length [Å] and angles [°] of Fc-azine.

C1-C6	1.454	C8-C7-N2	121.10
C7-C8	1.452	C7-N2-N1	111.60
C6-N1	1.282	C6-N2-N1	111.74
C7-N2	1.280	C1-C6-N1-N2	177.83
N1-N2	1.411	C8-C7-N2-N1	-179.38
C1-C6-N1	120.28	C6-N1-N2-C7	170.52

3. Results and discussion

By adding 1,1′-Ferrocenedicarboxaldehyde to an excess amount of hyrazinemonohydrate in methanol, FcDH was synthesized by a simple method in a high yield (93 %) for the first time [41]. As shown in Scheme 1, the reaction of FcDH with $Zn(OAc)_2{\cdot}2H_2O$ at 120 °C under high pressure led to the synthesis of uniformly dark-red crystals of Fc-azine. FT-IR spectrum of Fc-azine has shown a stretching band for the C=N group at 1628 cm ^{1} (Fig. 1, red curve), while the amine stretching band of FcDH at 3370 cm ^{1} (Fig. 1, black curve) completely disappeared. Raman spectrum of Fc-azine revealed characteristic bands for N—N stretching vibration at 997 cm ^{1} and symmetrical stretching band of C=N at 1569 cm ^{1}[36]. The TGA diagram revealed high thermal stability for Fc-azine and pseudo-one-step weight loss at 310–400 °C for oxidation of Cp rings and azine groups. The amount of final residual (40.8 % of initial mass ratio) is higher than the calculated amount for Fe_2O_3 (33.5 %) or Fe_3O_4 (32.3 %) as residue. According to the results of the EDS analysis, the higher amount of the residual is due to the presence of Zn-based derivatives on the surface of Fc-azine. In order to investigate the role of $Zn(OAc)_2{\cdot}2H_2O$, reactions were performed with catalytic amounts (1% mol) and in the absence of $Zn(OAc)_2{\cdot}2H_2O$. FT-IR spectrum of both reaction products (in the absence and using zincacetate in catalytic amount) demonstrated a sharp band for the C=N group at 1627 cm ^{1} and a suppressed band for the partly remaining amine functional group at 3418 cm ^{1} (Fig. 1, violet and green curve). However, Fc-azine is the main product at high temperatures; an equivalent amount of Zn $(OAc)_2{\cdot}2H_2O$ seems necessary to complete the reaction. The reaction of FcDH with the equivalent amount of acetic acid in the same condition also led to the same product as the reaction with the equivalent amount $Zn(OAc)_2{\cdot}2H_2O$ (Fig. 1, blue curve). Comparing the FT-IR spectra of the Fc-azine prepared using different amounts of $Zn(OAC)_2{\cdot}2H_2O$ (in the absence, mole ratio and also catalytic amount) revealed that Zn $(OAc)_2{\cdot}2H_2O$ could facilitate Fc-azine production by liberating acetic acid or dehydrogenation of the hydrazone group and, consequently, nitrogen molecule production [42–45].

3.1. Crystal structure of Fc-azine

Dark-red single crystals of Fc-azine were obtained directly from the reaction (Fig. 2a) mixture and used for crystal structure determination (Fig. 2b). Fc-azine crystallizes in the monoclinic space group $P2_1/c$ space group with two centrosymmetric molecules per unit cell. Tables 1 and 2 give crystal data and selected bond lengths and angles, respectively. The molecular structure of Fc-azine confirms the eclipsed conformation of Cp rings, which is common in ferrocene derivatives (Fig. 2c) [46–50]. The torsion angle of C6-N1-N2-C7 bonds (170.15) reveals a nearly planar structure for the azine bridge. Calculated dihedral angles (5.73 and 5.51°) confirm the nearly coplanar structure of the C6-N1-N2-C7 plane and Cp rings. The bond length of Fe-C (2.056 Å on average) is in the range reported for ferrocene derivatives. Bond lengths of C1-C6 (1.454 Å), C7-C8 (1.452 Å), C7-N2 (1.280 Å), C6-N1(1.282 Å), and N1-N2 (1.411 Å) are in agreement with reported C-C single bond, C=N double bond and N-N single bond of azine functional groups. The length of the C=N bond of Fc-azine is close to the reported C_{sp2}=N bond length (1.279 Å). Bond length for C1-C6, C7-C8, and N1-N2 are significantly shorter than the reported C_{sp2}—C_{sp2} (1.485 Å) and N-N (1.47 Å) single

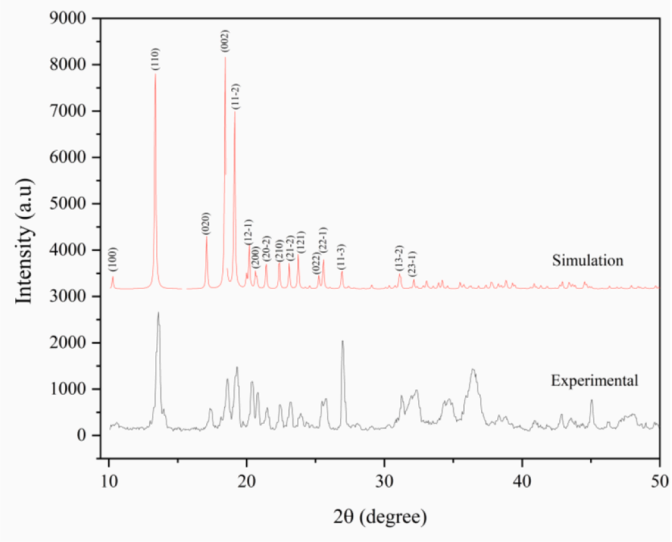

Fig. 3. Simulated and experimental powder XRD patterns of Fc-azine.

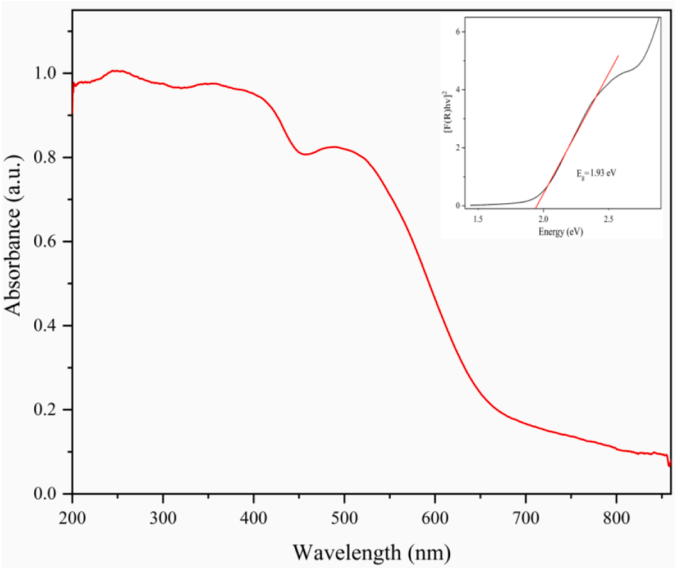

Fig. 4. UV–Vis Diffuse Reflectance spectrum (UV–Vis DRS) and band gap from Tauc plot (inset diagram) for Fcazine.

bonds, which could be due to possible conjugation of the Fc-zine molecule [51]. It has been found that the Fc-azine molecules contain off-center parallel intermolecular π-π interaction between C1-C2 (3.25 Å) and C3-C6 (3.36 Å), which were not observed for the other half of the molecule (C7-C12). It is also noteworthy that the experimental powder XRD pattern for Fc-azine is in good agreement with the simulated pattern on the base of the crystal structure obtained by single crystal diffraction (Fig. 3).

The crystallographic data (excluding structure factors) have been deposited with the Cambridge Crystallographic Data Centre (CCDC) as supplementary publication numbers CCDC-2341399. Copies of the data can be obtained, free of charge, by application to CCDC, 12 Union Road, Cambridge, CB2 1EZ, UK (Fax: +44 1223 336033; Email: data_request@ccdc.cam.ac.uk or via the internet: http://www.ccdc.cam.ac.uk/products/csd/request.

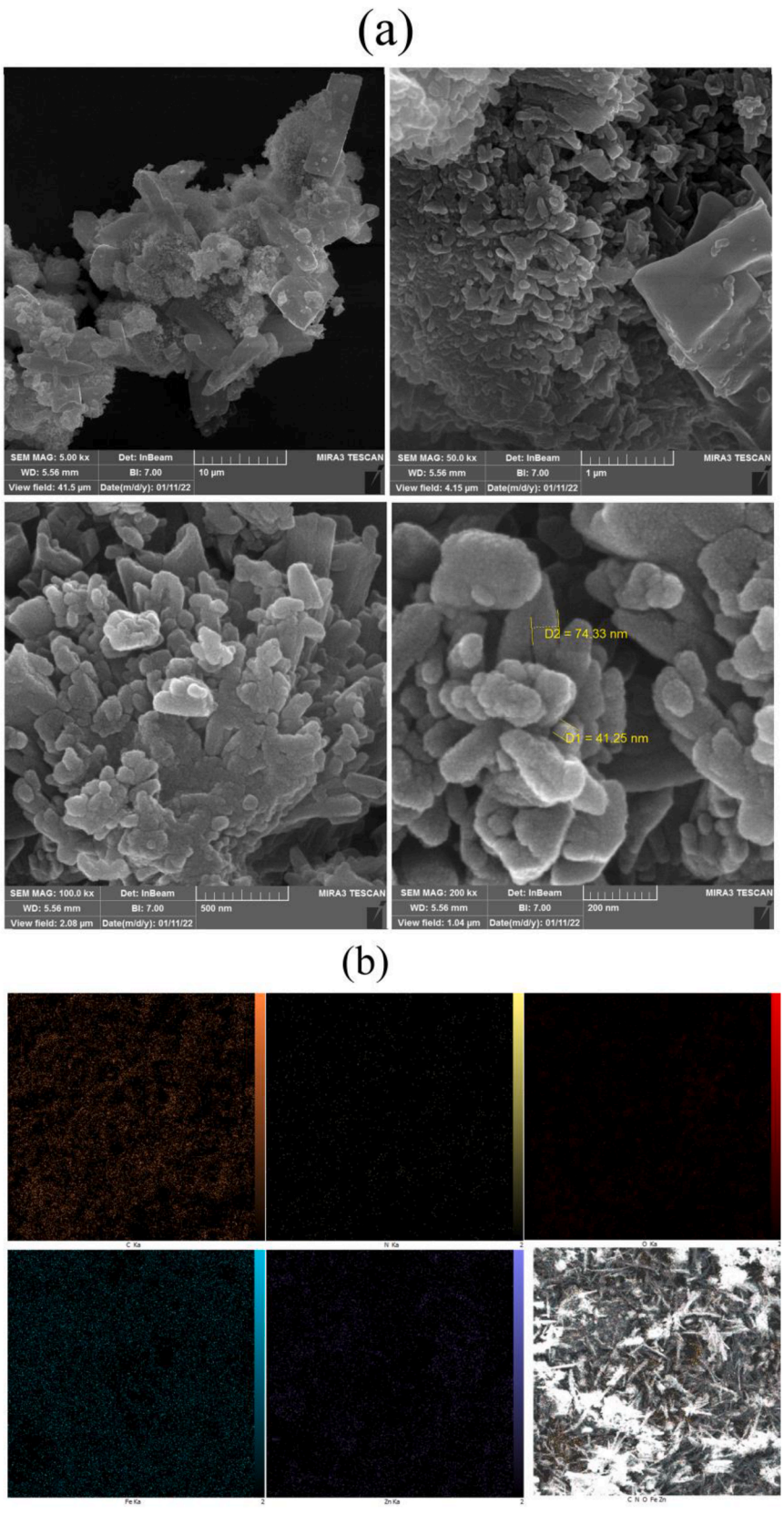

Fig. 5. (a) FE-SEM and (b) EDS map images of Fc-azine.

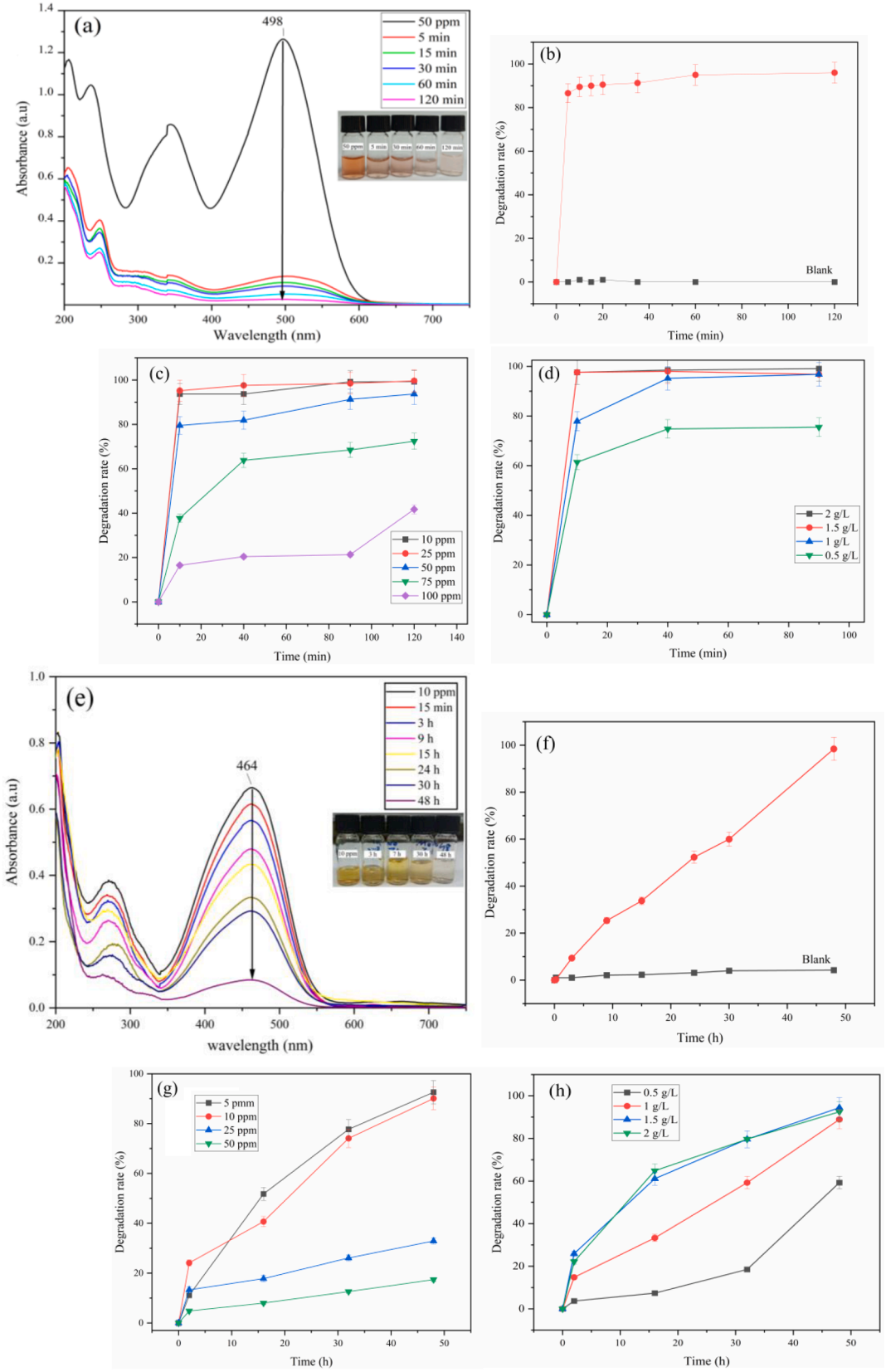

Fig. 6. (a) UV–Vis spectra of degradation of CR (50 ppm) by Fc-azine (1 g L^{-1}), (b) degradation rate of CR (50 ppm) in different time intervals by Fc-azine (1 g L^{-1}), (c) degradation of various concentration of CR by Fc-azine (1 g L^{-1}), (d) degradation of CR (50 ppm) with various amounts of Fc-azine, (e) UV–Vis spectra of degradation of MO (10 ppm) by Fc-azine (1 g L^{-1}), (f) degradation rate of MO (10 ppm) in different time intervals by Fc-azine (1 g L^{-1}), (g) degradation of various concentration of MO by Fc-azine (1 g L^{-1}), and (h) degradation of MO (10 ppm) with various amounts of Fc-azine.

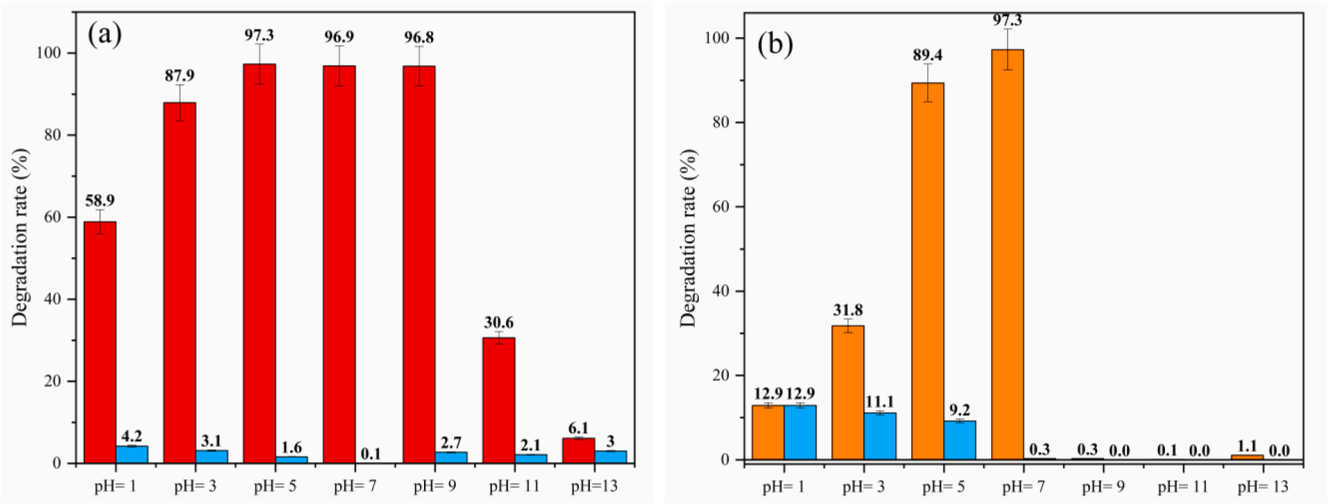

Fig. 7. Degradation of (a) CR (50 ppm) and (b) MO in different pH values by Fc-azine (1 g L^{-1}) in comparison blank experiments (blue bars).

3.2. UV–Vis Diffusive reflectance spectrum

Optical properties and relevant bond gap of Fc-azine were obtained from the UV–Vis Diffusive reflectance spectrum (Fig. 4) using Tauc and Kubelka-Munk functions (Eqs. (2) and (3)) [29].

$$(\alpha h\nu)^2 = A(h\nu \quad E_g) \tag{2}$$

$$\alpha \quad F(R) = \frac{(1 \quad R)^2}{2R} \tag{3}$$

Where α is the absorption coefficient, A is a constant, hν, Eg, and R are photon energy, the optical band gap, and reflectance, respectively. The Eg value for Fc-azine was 1.93 eV, in the range of reported catalysts used for AOP dye degradation in the dark [27,52,53].

3.3. Surface properties (BET measurement, zeta potential, FE-SEM and EDS map)

BET measurement of N_2 adsorption-desorption isotherm for Fc-azine was carried out at 77 K to examine porous structure. The calculated specific surface area, pore diameter, and pore volume were 19.12 m^2 g^{-1}, 15.1 nm, and 0.073 cm^3 g^{-1}, respectively. Zeta potential study revealed that the surface of Fc-zine is negatively charged (-17.6 mV) in water. FE-SEM image of Fc-azine (Fig. 5a) revealed a combination of regular-shaped and coral-shaped parts with non-uniform size (from 10 μm to 40 nm). EDS map (Fig. 5b) of Fc-azine confirmed the presence of Fe, C and N atoms of Fc-azine and Zn and O atoms as the remaining byproduct of $Zn(OAc)_2{\cdot}2H_2O$ on the surface of Fc-azine.

3.4. Azo dyes degradation study

Ferrocene as an electron donor and redox active molecule has been used to enhance degradation properties of AOP catalysts by optimizing band gap and producing active radicals through the Fenton-like reaction (where oxidation of Fe(II) to Fe(III) donated an electron to produce reactive oxygen species) [30–35]. In addition, an azine-based polymer with a π-conjugated system was reported to have good activity for aniline photocatalytic degradation [36]. Thus, the narrow band gap (1.93 eV), proper amount of specific surface area, presence of ferrocenyl groups, and possible conjugation through azine bridges of Fc-azine encouraged us to use it as an AOP catalyst. Interestingly, adding Fc-azine to an aqueous solution of dyes, including CR, MB, and MO, led to fast decoloring of CR. As shown in Fig. 6a, by the addition of Fc-azine to a 50 ppm solution of CR, the absorbance at 498 nm, as a characteristic absorbance for CR dye, decreased dramatically in 5 min. More than 86 % of CR was degraded in the first 5 min of the reaction, and degradation efficiency reached up to 96 % after 120 min in the dark (Fig. 6b). In the dark, different concentrations of CR from 10 to 100 ppm (Fig. 6c) were degraded by different amounts of Fc-Azine from 0.5 to 2 g L^{-1} (Fig. 6d). The optimum reaction condition was the degradation of a 50 ppm solution of CR with 1 g L^{-1} of Fc-azine [54,55]. No significant changes were observed for CR degradation efficiency in the presence of light (200-watt tungsten lamp). Very fast degradation of CR was not only confirmed by decreasing absorbance at 498 nm but also all absorbance at UV area (200–400 nm) corresponding to π-π* excitation of aromatic species were decreased [56]. Decolorization of MO solution (10 ppm) happened several hours after the reaction started, revealing the slow degradation of MO by Fc-azine. The characteristic absorbance of MO at 464 nm constantly decreased at a prolonged rate, and 98 % of MO degradation was obtained after 48 h (Fig. 6e and f). Degradation of MO in various concentrations from 5 to 50 ppm (Fig. 6g) was performed using different amounts of Fc-Azine from 0.5 to 2 g L^{-1} (Fig. 6h) in the dark. As a result, degradation of 10 ppm of MO solution by 1 g L^{-1} of Fc-azine was obtained as an optimum condition. Similar to CR degradation, absorbance at 270 nm for benzene rings of MO decreased alongside the absorbance at 464 nm, confirming the MO molecule's degradation. The addition of Fc-azine to the solution of MB dye did not lead to significant changes in its UV–Vis spectrum. The activity of Fc-azine for MO and CR as anionic dyes and inactivity for the degradation of MB as a cationic dye contrast with its negative surface charge, which could be associated with the dye degradation mechanism.

3.4.1. Effect of pH

Degradation of CR and MO by Fc-azine was performed in different acidic and basic environments, using HCl and NaOH as pH modifiers. FC-azine was able to degrade CR in the pH range of 5.0–9.0 without significant change in efficiency (Fig. 7a). The degradation rate decreased at pH values lower than 5.0 and decreased by almost 10 and 40 % at pH values 3 and 1, respectively. The probable protonation surface of Fc-azine or amine groups of CR and, consequently, disturbance of their interaction could be the reason for suppressing the activity of Fc-azine in the acidic environment [57]. In the basic environment, the degradation reaction was more affected due to the negative charge of the surface area of Fc-azine and its repulsion with CR as an anionic dye [58,59]. A similar result was observed for the degradation of MO in acidic and basic media (Fig. 7b). However, Fc-azine was completely deactivated for the degradation of MO in a basic environment. This result could be due to the weak interaction of MO with Fc-azine, which is interrupted entirely

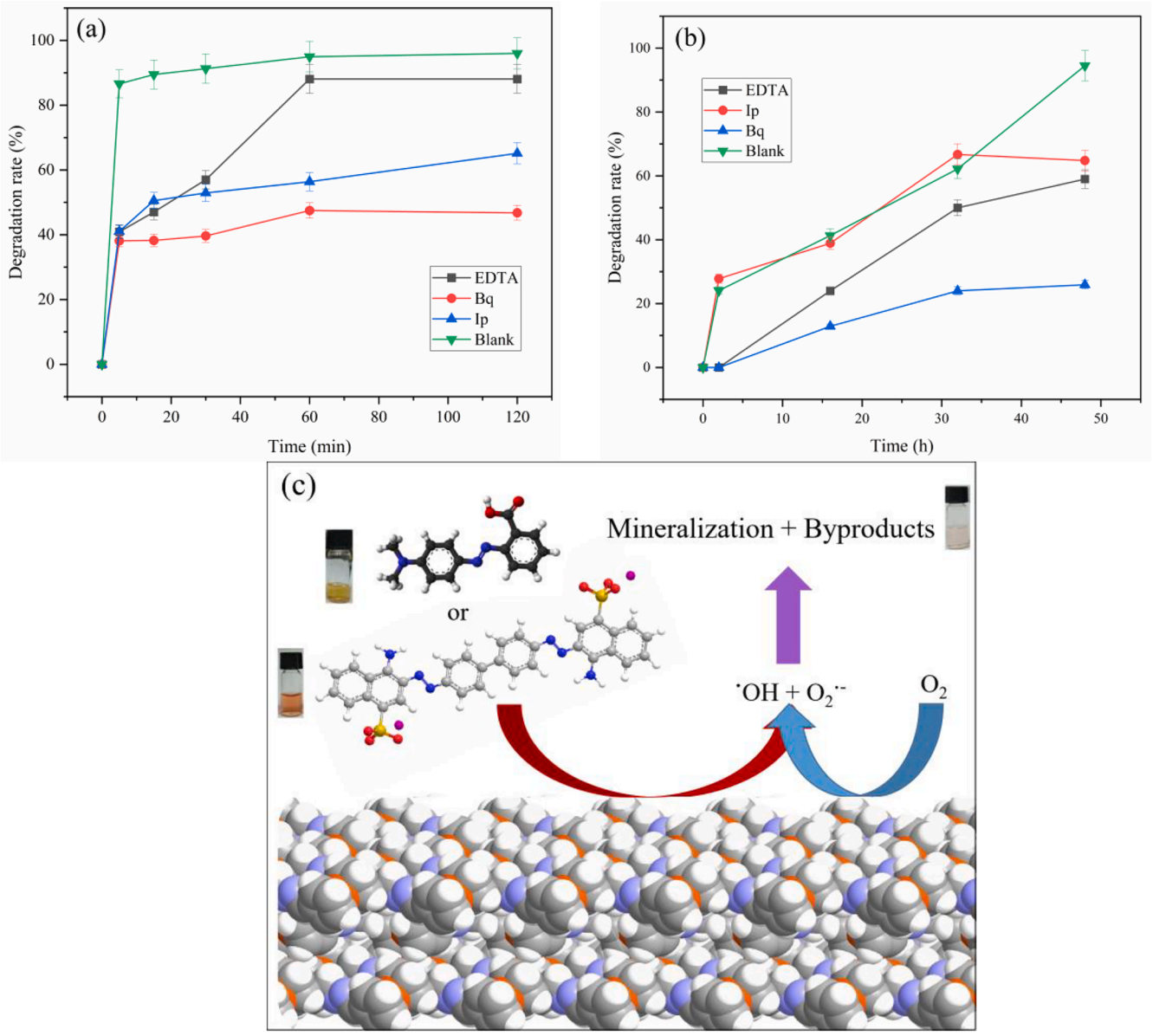

Fig. 8. Effect of Bq, EDTA and Ip as scavengers on the degradation rate of (a) CR (50 ppm) and (b) MO (10 ppm) by Fc-azine (1 g L^{-1}), and (c) schematic mechanism of CR and MO degradation by Fc-azine.

by increasing the negative charge of the surface of Fc-azine in basic pH values. In addition, it has been reported that ferrocene-based photocatalysts are more active in acidic media, the same as the Fenton reaction [32,60].

3.4.2. *Mechanism of degradation*

The possible degradation mechanism of CR and MO by Fc-azine was investigated by the addition of Ethylenediaminetetraacetic acid (EDTA), 1,4-benzoquinone (Bq) and isopropanol (Ip) at a concentration of 20 mM to the reaction mixtures as hole, superoxide anion ($O_2\cdot$) and hydroxyl radical (·OH) scavengers, respectively [5,61,62]. As demonstrated in Fig. 8a, the addition of scavengers suppressed CR degradation significantly. While the main part of CR was degraded during the first 5 min of the reaction, in the presence of EDTA, Bq and Ip, the degradation rate decreased to 81, 65 and 46 % after 2 h, respectively (Fig 8a). It has been reported that EDTA can disrupt the Fenton reaction by increasing the rate of radical quenching and can also lead to the stabilization of Fe (III) [63,64]. A similar effect of scavengers with a higher influence of Bq on the degradation of MO by Fc-azine was observed, confirming ROS production (·OH and $O_2\cdot$) and the AOP process (Fig. 8b). According to these results, both ·OH and $O_2\cdot$ species liberate during the reaction and play a crucial role in the degradation mechanism. It seems the adsorption of CR and MO dyes on the surface of Fc-azine led to the oxidation of Fe(II) to Fe(III), causing the release of electrons, which were captured by dissolved oxygen to produce superoxide anions. Also, the reduction of Fe (III) to Fe(II) by one-electron oxidation of CR and MO as anionic dyes possibly facilitated electron production by the ferrocenyl group [27, 65–68]. Produced $O_2\cdot$ as a reactive oxygen species can degrade dyes directly, or its further reactions lead to the production of ·OH, known as the most reactive free radical molecules. Eqs. (4)–(10)

$$\text{Dye (CR or MO)} + \text{Fc-azine} \longrightarrow \text{Fc-azine}^{\cdot+}(\text{Dye}_{ads}) + e^- \quad (4)$$

$$\text{Fc-azine}^{\cdot+}(\text{Dye}_{ads}) \longrightarrow \text{Dye}^{\cdot+} + \text{Fc-azine} \quad (5)$$

$$e^- + O_2 \longrightarrow O_2^{\cdot-} \quad (6)$$

$$O_2^{\cdot-} + H^+ \longrightarrow 2HO_2^{\cdot} \quad (7)$$

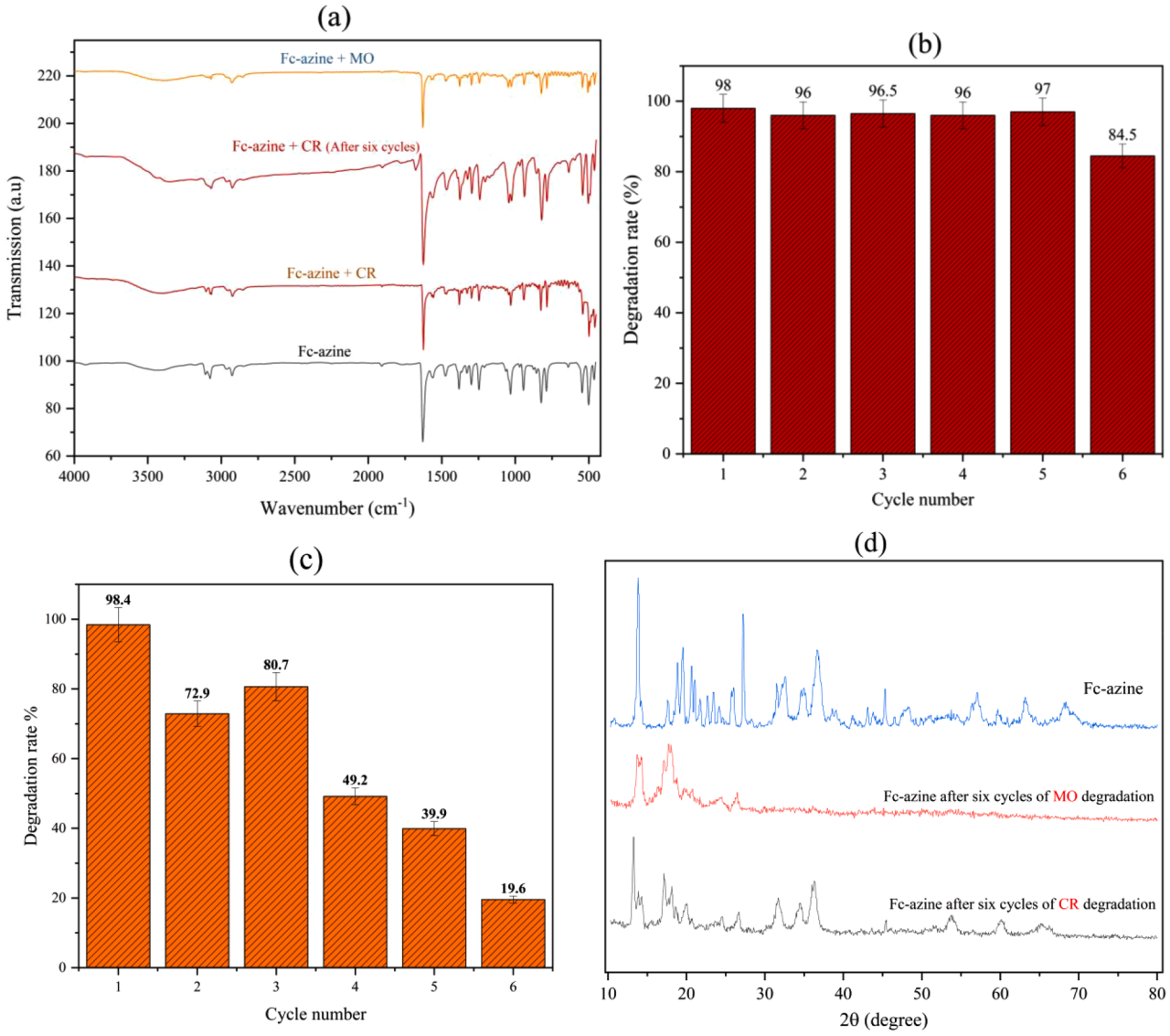

Fig. 9. (a) FT-IR spectra of Fc-azine (1 g L^{-1}) after MO (10 ppm) and CR (50 ppm) degradation, (b) reusability of the Fc-azine for CR degradation, (c) reusability of the Fc-azine for MO degradation, and (d) XRD patterns of Fc-azine after degradation of CR and MO.

$$2HO_2^{\cdot} \longrightarrow O_2 + H_2O_2 \quad (8)$$

$$H_2O_2 + e^- \longrightarrow OH^- + OH^{\cdot} \quad (9)$$

$$OH^{\cdot}/O_2^{\cdot-} + Dye^{\cdot+}/Dye \longrightarrow CO_2 + H_2O + byproduct \quad (10)$$

demonstrate reaction steps according to the proposed surface electron-transfer (SET) mechanism for the degradation of CR and MO by Fc-azine [3]. The schematic proposed mechanism of CR and MO degradation by Fc-Azine is illustrated in Fig. 8c. Based on the proposed mechanism, it seems that one-electron oxidation of CR or MO, as an anionic dye, plays a crucial role in the reaction mechanism. It is also in agreement with the negatively charged surface of Fc-azine and its inactivity for MB degradation as a cationic dye. It is worth mentioning that CR and MO are both anionic dyes, and the surface of Fc-azine is negatively charged. This is while the adsorption of dyes in the proposed mechanism plays an essential role in the degradation of CR and MO (Eqs. (4) and (5)). Thus, MO and CR could be adsorbed by π-π interaction of aromatics rings. The higher activity of Fc-azine for the degradation of CR is possibly due to the better interaction of CR with Fc-azine through the hydrogen bond between the amine groups of CR and the azine groups of Fc-azine [57,69–71].

3.4.3. *Adsorption, stability and reuse investigation*

In order to confirm that the removal of azo dyes is not only by surface adsorption, the FT-IR spectrum of Fc-azine was obtained after the degradation of CR and MO. As shown in Fig. 9a, no significant changes were observed in the FT-IR spectrum of Fc-azine before and after CR and MO removal. Furthermore, the reaction mixtures were centrifuged after the degradation, and Fc-azine was separated from the solution and dried at room temperature. By adding distilled water to recycled Fc-azine (10 mL per 0.01 g of Fc-azine), the suspension was sonicated for 1 h and centrifuged. Then, the concentration of CR and MO was determined by UV–Vis spectra of the aqueous phases. Only 8.8 % of the initial amount of CR was found to be adsorbed on the Fc-azine surface, and the adsorption of MO was negligible. Reusability and stability of Fc-azine were evaluated in six cycles of degradation of CR (Fig. 9b) and MO (Fig. 9c), confirming high stability and activity of Fc-azine for CR degradation even after six cycles (over 80 % after six cycles), which is one of the major conflicts of dark AOP catalysts. Fc-azine activity for degradation of MO was suppressed dramatically after three cycles. It seems a long time (48 h) degradation of MO led to the gradual

Table 3
Efficiency of some dark-ambient AOP catalysts for the degradation of azo dyes.

AOP Catalyst	Pollutant	Band gap (eV)	Reaction Condition & Efficiency	Recyclability and last cycle efficiency	Ref
$Cu_2O/(Ag0@Ag\text{-}NPs)_{0.15}$	Acid orange 7	1.33	Dye concentration: 200 ppm Catalyst loading: 1 g L^{-1} Efficiency: 94.4% in 2 h Additional source: Δ (30°C)	4^{th} cycle efficiency: ~70%	[28]
$Ca_{0.5}Sr_{0.5}Ni_{0.5}Cu_{0.5}O_{3-\delta}$	Orange (II)	-	Dye concentration: 20 ppm Catalyst loading: 1 g L^{-1} Efficiency: 90% in 2 h Additional source: none	15^{th} cycle efficiency: ~70%	[62]
$Ca_{0.75}Sr_{0.25}CuO_{3-\delta}$	Orange (II)	-	Dye concentration: 50 ppm Catalyst loading: 1 g L^{-1} Efficiency: 95% in 1 h Additional source: none	9^{th} cycle efficiency :~75%	[5]
CuAlLDH/MgO_2-50	Methyl orange	-	Dye concentration: 10 ppm Catalyst loading: 0.4 g L^{-1} Efficiency: 97% in 1 h Additional source: none	4^{th} cycle efficiency: ~92.7%	[4]
Fe_3O_4/MWCNT/SiO_2	Methylene blue	-	Dye concentration: 10 ppm Catalyst loading: 2 g L^{-1} Efficiency: 100% in 30 min Additional source: none	3^{rd} cycle efficiency: 44%	[11]
Mn(II) complexes	Rhodamine 6G & Congo red	1.8	Dye concentration: 10 ppm Catalyst loading: 2 g L^{-1} Efficiency: 99% in 40 min Additional source: none	6^{th} cycle efficiency: 97%	[52]
SnS	Congo red & Eriochrome black T & Methylene blue	2.07	Dye concentration: 40 ppm Catalyst loading: 1 g L^{-1} Efficiency: ~ 99 % in 60 min Additional source: none	4^{th} cycle efficiency: 37%	[27]
Fc-azine	Congo red & Methyl orange	1.93	Dye concentration: 50 ppm (CR) & 10 ppm (MO) Catalyst loading: 1 g L^{-1} Efficiency: 96 % in 2 h (CR) & 98% in 48 h (MO) Additional source: none	6^{th} cycle efficiency: 80%	This work

decomposition of Fc-azine. In order to investigate the stability of Fc-azine, the XRD pattern of Fc-azine was obtained after six cycles of CR and MO degradation (Fig. 9d). The XRD pattern of Fc-azine after degradation of MO revealed significant change due to the possible decomposition of FC-azine. Minor changes were observed in the XRD pattern of Fc-azine after CR degradation [72]. It is worth mentioning that over 80 % of Fc-azine has recovered after six cycles of CR degradation, and adsorption of CR was equal to 36 % of one cycle of reaction. Based on these results, Fc-azine is among the highly efficient and stable reported dark-ambient AOP catalysts for azo dye degradation (Table 3). Inductively coupled plasma atomic emission spectroscopy (ICP-AES) was used to determine the ion leaching of Fe and Zn during dye degradation. The measured concentrations of Fe and Zn ions of the reaction solution (after centrifugation) were 0.2 and 1.25 ppm, respectively.

3.4.4. Investigation of byproducts

In order to determine the possible byproducts of CR degradation, the reaction solution was extracted by n-hexane and diethyl ether and analyzed using the GC–MS technique. Two peaks at a retention time of 26.77 and 38.04 min with very weak intensity corresponding to fragments with M/Z = 386.2 and 400.2, respectively, were observed. It seems M/Z = 386. 07 is correspond to 3-([1,1′-biphenyl] 4-ylium-4′-yldiazenyl)naphthalene-1-sulfonate (calculated MW= 386.4 g mol^{-1}) and M/Z = 400.2 Correspond to 3-((4′-hydroxy-[1,1′-biphenyl] 4-yl) diazenyl) 4-nitrobenzenesulfonic acid (calculated MW = 399.05 g mol^{-1}). The appearance of a trace amount of these byproducts confirms not only the degradation of CR but also that the mineralization of CR proceeds at a high ratio.

4. Conclusion

Fc-azine was obtained from self-condensation of FcDH with using of $Zn(OAc)_2{\cdot}2H_2O$ or acetic acid at 120 °C and high pressure. Fc-azine, as a dark-ambient AOP catalyst, has shown high activity and stability (six efficient degradation cycles) for the rapid degradation of CR (80 % in 5 min) in slightly basic to acidic environments (pH= 5–9). Furthermore, Fc-azine can degrade MO in prolonged reaction time (98 % in 48 h) in natural or slightly acidic media (pH= 5–7). The effect of different scavengers on the degradation rate of MO and CR revealed the essential role of ·OH and O_2· in the degradation mechanism, confirming the AOP process. This result revealed high activity of Fc-azine compared to similar reported AOP catalysts in dark-ambient conditions. Based on our literature review, Fc-azine is the first ferrocene-based compound used for dye degradation in the dark without adding chemical reagents or external energy sources. These results could be a breakthrough in the design and synthesis of similar compounds for wastewater treatment.

Author statement

I have confirmed that this manuscript is original, has not been previously published, and is not currently under consideration for publication elsewhere. I confirm that all named authors have read and approved the manuscript and that no other individuals meet the authorship criteria but have not been listed. I also confirm that we all agreed on the order in which the authors are listed in the manuscript. I understand that the Corresponding Author is the main point of contact for the editorial process. The Corresponding Author is responsible for communicating with the other authors regarding progress, submission of revisions, and final approval of proofs.

CRediT authorship contribution statement

Shahriar Sharifi: Writing – review & editing, Writing – original draft, Visualization, Validation, Software, Investigation, Data curation, Conceptualization. **A. Wahid Mesbah:** Supervision, Writing – review & editing, Conceptualization, Validation, Resources. **Somayeh Golsanamlou:** Writing – review & editing, Validation, Methodology, Investigation, Data curation. **Aliakbar Tarlani:** Writing – review & editing, Validation, Resources, Methodology, Data curation. **Mitra Ghassemzadeh:** Writing – review & editing, Validation, Data curation. **Effat Iravani:** Writing – review & editing, Validation, Data curation. **Olaf Fuhr:** Writing – review & editing, Validation, Formal analysis, Data curation. **Dieter Fenske:** Writing – review & editing, Validation, Formal analysis.

Declaration of competing interest

The authors declare that they have no known competing financial interests or personal relationships that could have appeared to influence the work reported in this paper.

Data availability

Data will be made available on request.

Acknowledgment

This work was partly carried out with the support of the Karlsruhe Nano Micro Facility (KNMF), a Helmholtz Research Infrastructure at KIT.

References

[1] A. Pal, K.Y.H. Gin, A.Y.C. Lin, M. Reinhard, Impacts of emerging organic contaminants on freshwater resources: review of recent occurrences, sources, fate and effects, Sci. Total Environ. 408 (2010) 6062–6069, https://doi.org/10.1016/j.scitotenv.2010.09.026.

[2] D.J. Lapworth, N. Baran, M.E. Stuart, R.S. Ward, Emerging organic contaminants in groundwater: a review of sources, fate and occurrence, Environ. Pollut. 163 (2012) 287–303, https://doi.org/10.1016/j.envpol.2011.12.034.

[3] H. Chen, J. Ku, L. Wang, Thermal catalysis under dark ambient conditions in environmental remediation: fundamental principles, development, and challenges, Chin. J. Catal. 40 (2019) 1117–1134, https://doi.org/10.1016/S1872-2067(19)63366-8.

[4] S.G. Aragaw, G.B. Feysia, N.S. Gultom, D.H. Kuo, H. Abdullah, X. Chen, O. A. Zelekew, Synthesis of CuAl-layered double hydroxide/MgO_2 nanocomposite catalyst for the degradation of organic dye under dark condition, Appl. Water Sci. 12 (2022) 140, https://doi.org/10.1007/s13201-022-01668-6.

[5] H. Chen, J. Motuzas, W. Martens, J.C. Diniz da Costa, Degradation of azo dye Orange II under dark ambient conditions by calcium strontium copper perovskite, Appl. Catal. B Environ. 221 (2018) 691–700, https://doi.org/10.1016/j.apcatb.2017.09.056.

[6] S. Benkhaya, S. M'rabet, A. El Harfi, Classifications, properties, recent synthesis and applications of azo dyes, Heliyon 6 (2020), https://doi.org/10.1016/j.heliyon.2020.e03271 e03271.

[7] R. Kant, Textile dyeing industry an environmental hazard, NS 04 (2012) 22–26, https://doi.org/10.4236/ns.2012.41004.

[8] S. Wijetunga, X.F. Li, C. Jian, Effect of organic load on decolourization of textile wastewater containing acid dyes in upflow anaerobic sludge blanket reactor, J. Hazard. Mater. 177 (2010) 792–798, https://doi.org/10.1016/j.jhazmat.2009.12.103.

[9] L.P.V.V. Rajagopalan, A new synergetic nanocomposite for dye degradation in dark and light, Sci. Rep. 6 (2016) 38606, https://doi.org/10.1038/srep38606.

[10] R. Al-Tohamy, S.S. Ali, F. Li, K.M. Okasha, Y.A.G. Mahmoud, T. Elsamahy, H. Jiao, Y. Fu, J. Sun, A critical review on the treatment of dye-containing wastewater: ecotoxicological and health concerns of textile dyes and possible remediation approaches for environmental safety, Ecotoxicol. Environ. Saf. 231 (2022) 113160, https://doi.org/10.1016/j.ecoenv.2021.113160.

[11] E. Molahosseini, M. Molaei, H. Zare, F. Farahmandzadeh, A novel dark catalyst material based on Fe_3O_4/MWCNT/SiO_2 magnetic nanocomposite for simple and ultrafast degradation of methylene blue, Mater. Res. Bull. 170 (2024) 112571, https://doi.org/10.1016/j.materresbull.2023.112571.

[12] C. Zhang, Y. Li, M. Li, D. Shuai, X. Zhou, X. Xiong, C. Wang, Q. Hu, Continuous photocatalysis via photo-charging and dark-discharging for sustainable environmental remediation: performance, mechanism, and influencing factors, J. Hazard. Mater. 420 (2021) 126607, https://doi.org/10.1016/j.jhazmat.2021.126607.

[13] A. Soltani, M. Faramarzi, S.A. Mousavi Parsa, A review on adsorbent parameters for removal of dye products from industrial wastewater, Water Qual. Res. J. 56 (2021) 181–193, https://doi.org/10.2166/wqrj.2021.023.

[14] B. Dayı, C. Onac, A. Kaya, H.A. Akdogan, S. Rodriguez-Couto, New type biomembrane: transport and biodegradation of reactive textile dye, ACS Omega 5 (2020) 9813–9819, https://doi.org/10.1021/acsomega.9b04433.

[15] K.T. Chung, C.E. Cerniglia, Mutagenicity of azo dyes: structure-activity relationships, Mutat. Res. Rev. Genet. Toxicol. 277 (1992) 201–220, https://doi.org/10.1016/0165-1110(92)90044-A.

[16] A. Boretti, L. Rosa, Reassessing the projections of the World Water Development Report, npj Clean Water 2 (2019) 15, https://doi.org/10.1038/s41545-019-0039-9.

[17] S.V. Besegatto, A. Da Silva, C.E.M. Campos, S.M.A.G.U. De Souza, A.A.U. De Souza, S.Y.G. González, Perovskite-based Ca-Ni-Fe oxides for azo pollutants fast abatement through dark catalysis, Appl. Catal. B Environ. 284 (2021) 119747, https://doi.org/10.1016/j.apcatb.2020.119747.

[18] A. Fujishima, K. Honda, Electrochemical photolysis of water at a semiconductor electrode, Nature 238 (1972) 37–38, https://doi.org/10.1038/238037a0.

[19] A. Ajmal, I. Majeed, R.N. Malik, H. Idriss, M.A. Nadeem, Principles and mechanisms of photocatalytic dye degradation on TiO_2 based photocatalysts: a comparative overview, RSC Adv. 4 (2014) 37003–37026, https://doi.org/10.1039/C4RA06658H.

[20] E. Alimohammadi, V. Mahdikhah, S. Sheibani, Type-II band alignment in CNT-modified $SrTiO_3$-Fe_2TiO_5 heterostructure nanocomposite for photocatalytic degradation of organic dyes, Appl. Surf. Sci. 598 (2022) 153816, https://doi.org/10.1016/j.apsusc.2022.153816.

[21] E. Montakhab, F. Rashchi, S. Sheibani, Enhanced photocatalytic activity of TiO_2 nanotubes decorated with Ag nanoparticles by simultaneous electrochemical deposition and reduction processes, Appl. Surf. Sci. 615 (2023) 156332, https://doi.org/10.1016/j.apsusc.2023.156332.

[22] S. Gautam, H. Agrawal, M. Thakur, A. Akbari, H. Sharda, R. Kaur, M. Amini, Metal oxides and metal organic frameworks for the photocatalytic degradation: a review, J. Environ. Chem. Eng. 8 (2020) 103726, https://doi.org/10.1016/j.jece.2020.103726.

[23] Z. Stasicka, Chapter 7 - Transition metal complexes as solar photocatalysts in the environment: a short review of recent development, R. van Eldik, G. Stochel (Eds.). Advances in Inorganic Chemistry, Academic Press, 2011, pp. 291–343, https://doi.org/10.1016/B978-0-12-385904-4.00004-4.

[24] A. Abramov, S. Bonardd, R. Pérez-Ruiz, D. Díaz Díaz, Recyclable, immobilized transition-metal photocatalysts, Adv. Synth. Catal. 364 (2022) 2–17, https://doi.org/10.1002/adsc.202101048.

[25] Mg Magnetic, Fe_2O_4–$CaFe_2O_4$ S-scheme photocatalyst prepared from recycling of electric arc furnace dust, J. Environ. Manag. 290 (2021) 112609, https://doi.org/10.1016/j.jenvman.2021.112609.

[26] The enhanced photocatalytic activity of ZnO nanorods/CuO nanourchins composite prepared by chemical bath precipitation, Mater. Sci. Eng. B 271 (2021) 115262, https://doi.org/10.1016/j.mseb.2021.115262.

[27] S. Jayaraman, A.R. Warrier, Dark catalytic degradation of industrial dye effluents using orthorhombic Tin monosulphide nanocatalyst, J. Mol. Liq. 301 (2020) 112360, https://doi.org/10.1016/j.molliq.2019.112360.

[28] X. Wan, J. Yang, X. Huang, S. Tie, S. Lan, A high-performance room temperature thermocatalyst Cu_2O/Ag_0@Ag-NPs for dye degradation under dark condition, J. Alloy. Compd. 785 (2019) 398–409, https://doi.org/10.1016/j.jallcom.2019.01.215.

[29] A.F. Cabrera, C.E. Rodríguez Torres, S.G. Marchetti, S.J. Stewart, Degradation of methylene blue dye under dark and visible light conditions in presence of hybrid composites of nanostructured $MgFe_2O_4$ ferrites and oxygenated organic compounds, J. Environ. Chem. Eng. 8 (2020), https://doi.org/10.1016/j.jece.2020.104274, 104274.

[30] Z. Huang, H. Yu, L. Wang, M. Wang, X. Liu, D. Shen, S. Shen, S. Ren, T. Lin, S. Lei, Ferrocene doped ZIF-8 derived Fe-N-C single atom catalyst to active peroxymonosulfate for removal of bisphenol A, Sep. Purif. Technol. 305 (2023) 122402, https://doi.org/10.1016/j.seppur.2022.122402.

[31] Y. Li, B. Zhang, X. Liu, Q. Zhao, H. Zhang, Y. Zhang, P. Ning, S. Tian, Ferrocene-catalyzed heterogeneous Fenton-like degradation mechanisms and pathways of antibiotics under simulated sunlight: a case study of sulfamethoxazole, J. Hazard. Mater. 353 (2018) 26–34, https://doi.org/10.1016/j.jhazmat.2018.02.034.

[32] K.Y.A. Lin, J.T. Lin, Ferrocene-functionalized graphitic carbon nitride as an enhanced heterogeneous catalyst of Fenton reaction for degradation of Rhodamine B under visible light irradiation, Chemosphere 182 (2017) 54–64, https://doi.org/10.1016/j.chemosphere.2017.04.152.

[33] Y. Nie, C. Hu, J. Qu, X. Hu, Efficient photodegradation of Acid Red B by immobilized ferrocene in the presence of UVA and H_2O_2, J. Hazard. Mater. 154 (2008) 146–152, https://doi.org/10.1016/j.jhazmat.2007.10.005.

[34] Z. Wang, H. Wang, Z. Wang, D. Huang, H. Qin, Y. He, M. Chen, G. Zeng, P. Xu, Ferrocene modified g-C_3N_4 as a heterogeneous catalyst for photo-assisted activation of persulfate for the degradation of tetracycline, Colloids Surf. A

Physicochem. Eng. Asp. 626 (2021) 127024, https://doi.org/10.1016/j.colsurfa.2021.127024.
[35] M.W. Zhang, M.T. Yang, S. Tong, K.Y.A. Lin, Ferrocene-modified iron-based metal-organic frameworks as an enhanced catalyst for activating oxone to degrade pollutants in water, Chemosphere 213 (2018) 295–304, https://doi.org/10.1016/j.chemosphere.2018.09.051.
[36] T. Kotnik, G. Žerjav, A. Pintar, E. Žagar, S. Kovačič, Azine- and imine-linked conjugated polyHIPEs through Schiff-base condensation reaction, Polym. Chem. 13 (2022) 474–478, https://doi.org/10.1039/D1PY01467F.
[37] G.G.A. Balavoine, G. Doisneau, T. Fillebeen-Khan, An improved synthesis of ferrocene-1,1′-dicarbaldehyde, J. Organomet. Chem. 412 (1991) 381–382, https://doi.org/10.1016/0022-328X(91)86082-2.
[38] O.V. Dolomanov, L.J. Bourhis, R.J. Gildea, J.A.K. Howard, H. Puschmann, OLEX2: a complete structure solution, refinement and analysis program, J. Appl. Crystallogr. 42 (2009) 339–341, https://doi.org/10.1107/S0021889808042726.
[39] G.M. Sheldrick, SHELXT – Integrated space-group and crystal-structure determination, Acta Crystallogr. A 71 (2015) 3–8, https://doi.org/10.1107/S2053273314026370.
[40] G.M. Sheldrick, Crystal structure refinement with SHELXL, Acta Crystallogr. C 71 (2015) 3–8, https://doi.org/10.1107/S2053229614024218.
[41] S. Sharifi, A. Wahid Mesbah, E. Iravani, A new unsymmetrical ferrocene-based double azine as a multichannel chemosensor for the detection of Cu^{2+} ions, Results Chem. 5 (2023) 100747, https://doi.org/10.1016/j.rechem.2022.100747.
[42] D.D. Hile, H.C. Swart, S.V. Motloung, T.E. Motaung, K.O. Egbo, L.F. Koao, Effect of hydrazine hydrate as complexing agent in the synthesis of zinc selenide thin films by chemical bath deposition, Thin Solid Films 693 (2020) 137707, https://doi.org/10.1016/j.tsf.2019.137707.
[43] A. Stojiljković, N. Orbović, S. Sredojević, M.L.J. Mihailović, The reaction of lead tetraacetate with unsubstituted hydrazones of some aromatic ketones and aldehydes, Tetrahedron 26 (1970) 1101–1107, https://doi.org/10.1016/S0040-4020(01)98787-3.
[44] X. Liu, Y. Xiang, X. Ma, G. Ren, L. Gao, Ferrocene macrocyclic schiff base complex: synthesis, structure and recognition properties for dual Hg^{2+} and Cu^{2+}, Russ. J. Gen. Chem. 87 (2017) 2986–2988, https://doi.org/10.1134/S1070363217120428.
[45] T.L. Holton, H. Schechter, Advantageous syntheses of diazo compounds by oxidation of hydrazones with lead tetraacetate in basic environments, J. Org. Chem. 60 (1995) 4725–4729, https://doi.org/10.1021/jo00120a013.
[46] A.G. Osborne, M. Webba da Silva, M.B. Hursthouse, K.M.A. Malik, G. Opromolla, P. Zanello, Synthetic, structural and electrochemical studies on some ferrocenylazines: crystal structures of [4](1) (1,4-dimethyl-2,3-diazabuta-1,3-dien) ferrocenophane and [42](1,1′) bis(1,4-dimethyl-2,3-diazabuta-1,3-dien) ferrocenophane, J. Organomet. Chem. 516 (1996) 167–176, https://doi.org/10.1016/0022-328X(96)06138-4.
[47] N. Mouas Toma, H. Merazig, J.C. Daran, É. Manoury, Synthesis and characterization of new ferrocenyl bishydrazones, C. R. Chim. 18 (2015) 801–807, https://doi.org/10.1016/j.crci.2015.06.002.
[48] M. Emirik, K. Karaoğlu, K. Serbest, U. Çoruh, E.M. Vazquez Lopez, Two novel unsymmetrical ferrocene based azines and their complexing abilities towards Cu (II): spectroscopy, crystal structure, electrochemistry and DFT calculations, Polyhedron 88 (2015) 182–189, https://doi.org/10.1016/j.poly.2014.12.044.
[49] K. Karaoğlu, K. Serbest, M. Emirik, E. Şahin, An unsymmetrical ferrocene based azine and its Cu(II) complex: spectroscopy, crystal structure, electrochemistry and DFT calculations, J. Organomet. Chem. 775 (2015) 80–87, https://doi.org/10.1016/j.jorganchem.2014.10.021.
[50] X.Q. Hao, J.F. Gong, W.T. Song, Y.J. Wu, M.P. Song, Synthesis and crystal structures of mono-, bis- as well as tris-mercurated complexes with ferrocenylazines, Inorg. Chem. Commun. 10 (2007) 371–375, https://doi.org/10.1016/j.inoche.2006.11.014.
[51] J. Dong, Y. Liu, J. Hu, Q. Teng, J. Cheng, Y. Luo, H. Zhang, Synthesis of ferrocenyl-based unsymmetrical azines via a simple reaction of aldehydes with ketone-derived *N* -tosyl hydrazones and the evaluation of the extent of conjugation in the molecule, Organometallics 36 (2017) 3215–3225, https://doi.org/10.1021/acs.organomet.7b00366.
[52] R. Vallavoju, R. Kore, R.P.M. Subburu, M. Basude, P. Chetti, S. Pola, Degradation of organic pollutants in the presence of new Mn (II) complexes under ambient light or darkness conditions, J. Photochem. Photobiol. A Chem. 442 (2023) 114775, https://doi.org/10.1016/j.jphotochem.2023.114775.
[53] D.S. Pan, K.B. Chu, L.L. Zhou, Z.H. Guo, J.L. Song, $(C_5H_9N_2)[BiI_4]$: a one-dimensional bismuth-based organic–inorganic hybrid material for fast rhodamine B degradation under dark condition, J. Clust. Sci. 33 (2022) 1205–1210, https://doi.org/10.1007/s10876-021-02055-y.
[54] F. Yu, B. Guo, Y. Zhuang, S. Komarneni, J. Ma, Degradation of tetracycline by activating persulfate with $ZnFe_2O_4$-Bi_2MoO_6 catalyst under visible light, Mater. Today Commun. 36 (2023) 106460, https://doi.org/10.1016/j.mtcomm.2023.106460.
[55] L. Gong, Z. Yao, C. Zhu, X. Lian, B. He, L. Qu, W. Xiong, B. Yu, Synthesis of porous $Mg(OH)_2$ nanowires for phosphate removal from water, Colloids Surf. A Physicochem. Eng. Asp. 676 (2023) 132137, https://doi.org/10.1016/j.colsurfa.2023.132137.
[56] H. Chen, J. Motuzas, W. Martens, J.C. Diniz da Costa, Surface and catalytic properties of stable Me(Ba, Ca and Mg)SrCoO for the degradation of orange II dye under dark conditions, Appl. Surf. Sci. 450 (2018) 292–300, https://doi.org/10.1016/j.apsusc.2018.04.193.
[57] S. Wei, X. Hu, H. Liu, Q. Wang, C. He, Rapid degradation of Congo red by molecularly imprinted polypyrrole-coated magnetic TiO_2 nanoparticles in dark at ambient conditions, J. Hazard. Mater. 294 (2015) 168–176, https://doi.org/10.1016/j.jhazmat.2015.03.067.
[58] L. Zhu, S. Zhou, H. Cheng, S. Komarneni, J. Ma, *In-situ* growth of Mn-Ni_3S_2 on nickel foam for catalytic ozonation of p-nitrophenol, Chemosphere 357 (2024) 142037, https://doi.org/10.1016/j.chemosphere.2024.142037.
[59] S. Zhou, F. Zhu, H. Cheng, S. Komarneni, J. Ma, *In-situ* growth of Ni_3S_2@Mo_2S_3 catalyst on Mo-Ni foam for degradation of p-nitrophenol with a good synergetic effect by using ozone, J. Environ. Chem. Eng. 11 (2023) 111477, https://doi.org/10.1016/j.jece.2023.111477.
[60] Q. Wang, S. Tian, P. Ning, Degradation mechanism of methylene blue in a heterogeneous fenton-like reaction catalyzed by ferrocene, Ind. Eng. Chem. Res. 53 (2014) 643–649, https://doi.org/10.1021/ie403402q.
[61] H. Chen, T. Cai, W. Dong, J. Wang, Y. Liu, W. Li, X. Xia, L. Tang, Catalytic thermal degradation of tetracycline based on iron-based MOFs and annealed derivative in dark condition, J. Clean. Prod. 406 (2023) 136976, https://doi.org/10.1016/j.jclepro.2023.136976.
[62] H. Chen, J. Motuzas, W. Martens, J.C. Diniz Da Costa, Effective degradation of azo dyes in the dark by Cu^{2+} active sites in CaSrNiCu oxides, J. Environ. Chem. Eng. 6 (2018) 5870–5878, https://doi.org/10.1016/j.jece.2018.08.060.
[63] B.S. Aytar, J.P.E. Muller, S. Golan, Y. Kondo, Y. Talmon, N.L. Abbott, D.M. Lynn, Chemical oxidation of a redox-active, ferrocene-containing cationic lipid: influence on interactions with DNA and characterization in the context of cell transfection, J. Colloid Interface Sci. 387 (2012) 56–64, https://doi.org/10.1016/j.jcis.2012.07.083.
[64] L. Li, Y. Abe, K. Kanagawa, T. Shoji, T. Mashino, M. Mochizuki, M. Tanaka, N. Miyata, Iron-chelating agents never suppress Fenton reaction but participate in quenching spin-trapped radicals, Anal. Chim. Acta 599 (2007) 315–319, https://doi.org/10.1016/j.aca.2007.08.008.
[65] C.M. Magdalane, G.M.A. Priyadharsini, K. Kaviyarasu, A.I. Jothi, G.G. Simiyon, Synthesis and characterization of TiO_2 doped cobalt ferrite nanoparticles via microwave method: investigation of photocatalytic performance of congo red degradation dye, Surf. Interfaces 25 (2021) 101296, https://doi.org/10.1016/j.surfin.2021.101296.
[66] M.Y. Leiw, G.H. Guai, X. Wang, M.S. Tse, C.M. Ng, O.K. Tan, Dark ambient degradation of Bisphenol A and Acid Orange 8 as organic pollutants by perovskite $SrFeO_3$ δ metal oxide, J. Hazard. Mater. 260 (2013) 1–8, https://doi.org/10.1016/j.jhazmat.2013.04.031.
[67] H. Chen, J. Motuzas, W. Martens, J.C. Diniz da Costa, Degradation of orange II dye under dark ambient conditions by MeSrCuO (Me = Mg and Ce) metal oxides, Sep. Purif. Technol. 205 (2018) 293–301, https://doi.org/10.1016/j.seppur.2018.05.029.
[68] Catalyzed degradation of azo dyes under ambient conditions, Environ. Sci. Technol. (2024), https://doi.org/10.1021/es1027234 (n.d.) accessed February 13.
[69] J.W. Heo, L. An, J. Chen, J.H. Bae, Y.S. Kim, Preparation of amine-functionalized lignins for the selective adsorption of Methylene blue and Congo red, Chemosphere 295 (2022) 133815, https://doi.org/10.1016/j.chemosphere.2022.133815.
[70] K. Li, H. Zhang, C. Chang, K. Lin, B. Zhang, Z. Ma, D. Wei, Q. Zhang, A hydrogen bonded azine as a building block for π-conjugated polymers and their semiconducting properties, Polym. Chem. 15 (2024) 991–998, https://doi.org/10.1039/D3PY01346D.
[71] S. Liu, Y. Ding, P. Li, K. Diao, X. Tan, F. Lei, Y. Zhan, Q. Li, B. Huang, Z. Huang, Adsorption of the anionic dye Congo red from aqueous solution onto natural zeolites modified with N,N-dimethyl dehydroabietylamine oxide, Chem. Eng. J. 248 (2014) 135–144, https://doi.org/10.1016/j.cej.2014.03.026.
[72] Activation of $Na_2S_2O_8$ by MIL-101(Fe)/MoS_2 composite for the degradation of tetracycline with visible light assistance, Colloids Surf. A Physicochem. Eng. Asp. 654 (2022) 130202, https://doi.org/10.1016/j.colsurfa.2022.130202.